Journal of Alloys and Compounds 500 (2010) 181–184

Contents lists available at ScienceDirect

Journal of Alloys and Compounds

journal homepage: www.elsevier.com/locate/jallcom

Influence of cooling rate on optical properties and electrical properties of nanorod ZnO films

Meizhen Gao*, Jing Liu, Huina Sun, Xiaonan Wu, Desheng Xue

Key Lab for Magnetism and Magnetic Materials of MOE, Lanzhou University, Lanzhou 730000, China

ARTICLE INFO

Article history:
Received 19 January 2010
Received in revised form 23 March 2010
Accepted 30 March 2010
Available online 8 April 2010

Keywords:
ZnO
Cooling rate
Oxygen vacancies
Electrical property
Optical property

ABSTRACT

ZnO films are prepared on Ag-coated glass substrates by wet chemical method at low temperature using $Zn(NO_3)\cdot 6H_2O$ and dimethylamine borane complex (DMAB). The structural, electrical and optical properties of ZnO films are investigated by X-ray diffraction, scanning electron microscope, four-point probe method and photoluminescence, respectively. The ZnO film deposited at 90 °C is the most compact films with a *c*-axis preferred orientation. The cooling rate affects the optical and electrical properties of ZnO films dramatically. The ZnO films cooled at −15 °C exhibit the lowest electrical resistivity of 0.525 Ω cm and the strongest photoluminescence in visible light. The increase of the conductivity and the enhancement of the photoluminescence are attributed to the increase of oxygen vacancies in the films.

1. Introduction

Zinc oxide (ZnO), a representative II–VI group compound semiconductor, has a direct wide bandgap of 3.37 eV and a large exciton binding energy of 60 meV, a low power threshold for optical pumping, and a high transmittance of visible light about 80% at room temperature. Therefore, lots of investigations have been done on ZnO films in order to apply these films to practical applications, such as, solar cells [1], photo detectors [2], light-emitting devices [3], thin film transistors [4], and surface acoustic wave guides [5].

There are several methods that can be used to prepare ZnO films, such as sputtering [6], pulsed laser deposition [7], chemical vapor deposition [8], molecular beam epitaxy [9], and sol–gel process [10], etc. However, these methods are not well suited for large area coating, low temperature processing, and low cost. In this work, we choose a simple and low-cost method—wet chemical preparation to prepare the ZnO films on large area substrates at a low temperature [11].

It is well known that concentration of oxygen vacancies has a great influence on optical and electrical properties of ZnO films. Moreover, it is very difficult to control the concentration of oxygen vacancies in the ZnO films by modulating the growth and thermal treatment conditions. In this work, the ZnO films are obtained on Ag-catalyzed substrates by low-temperature wet chemical method. The influence of oxygen vacancies on optical and electrical properties of ZnO films are studied by comparative measurements of electrical conductivity and photoluminescence (PL) of ZnO films. A low resistivity of 0.525 Ω cm has been obtained.

2. Experimental procedures

2.1. Synthesis of nanorod ZnO films

Prior to deposition, glass substrates were cleaned ultrasonically in ethanol and acetone for removing organic impurities and rinsed in distilled water. Ag layer was deposited on the glass substrate using a two-step Sn/Ag activation process at room temperature [12]. Subsequently, the Ag-coated glass substrates were immersed into aqueous solution at 70 °C, 80 °C, 90 °C, respectively, which contains 0.05 M zinc nitrate hexahydrate [$Zn(NO_3)\cdot 6H_2O$] and 0.05 M dimethylamine borane complex (DMAB) [$(CH_3)_2NHBH_3$]. The films were taken out after 1 h, and annealed at 500 °C in air for 1 h. After annealing, the films were cooled (i) in furnace, (ii) in air, (iii) at −15 °C. Three samples were characterized for each preparation parameter set.

2.2. Characterization

The crystal structure of the ZnO films was characterized by using an X-ray diffractometer (Philips X' Pert Pro with Cu Kα, 0.154056 nm). The surface morphology and cross-section of the films were observed by a field emission scanning electron microscope (FE-SEM, Hitachi S-4800). The sheet resistance was measured by four-point probe method (SX1934 digital four-point testing instrument, $0–2\times10^6$ Ω/□). The photoluminescence was obtained by using a He–Cd laser with 325 nm wavelength as excitation source.

3. Results and discussion

Fig. 1 shows the surface and cross-section morphologies of the ZnO films. From Fig. 1, we can see that all films present regular hexagonal nanorods. The average diameters of ZnO nanorods

* Corresponding author. Fax: +86 931 8913554.
E-mail address: gaomz@lzu.edu.cn (M. Gao).

0925-8388/$ – see front matter © 2010 Elsevier B.V. All rights reserved.
doi:10.1016/j.jallcom.2010.03.236

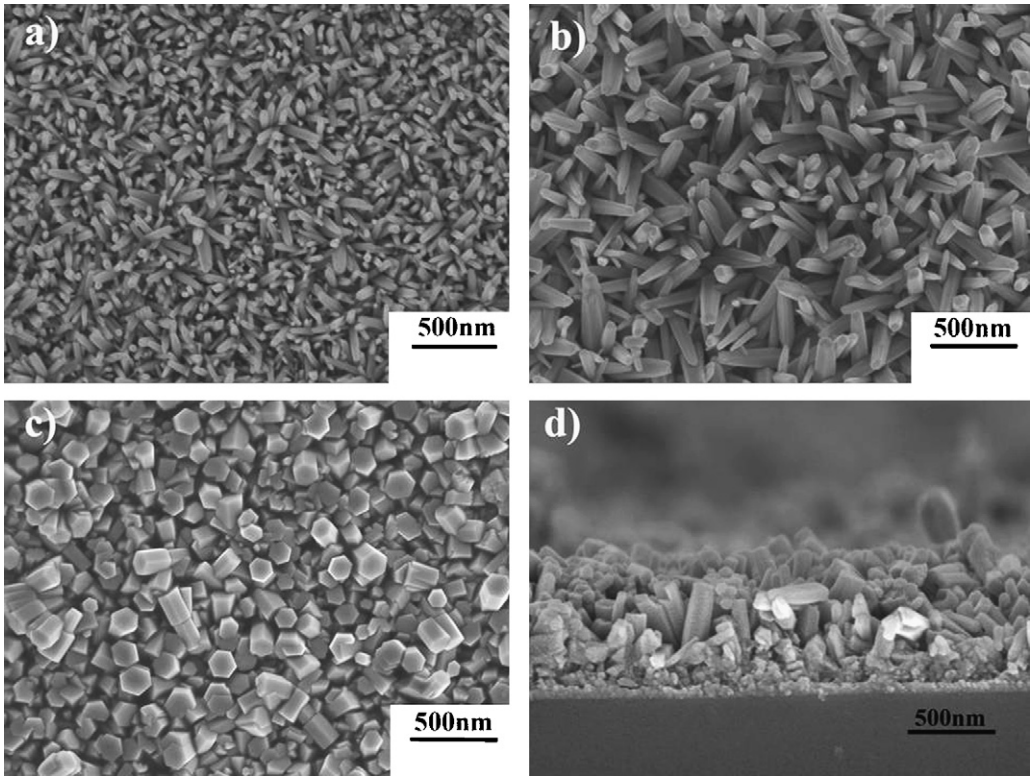

Fig. 1. SEM images of the morphology of ZnO films at different deposition temperature for 1 h: (a) 70 °C, (b) 80 °C, (c) 90 °C, and (d) the cross-section of the ZnO film deposited at 90 °C.

deposited at 70 °C, 80 °C and 90 °C are 40 nm, 60 nm, and 100 nm, respectively. The compaction of the ZnO films increases with increasing temperature. The film deposited at 90 °C holds the highest degree of compaction. We think the enhanced compaction is due to a more sufficient growth of the nanorods with increasing deposition temperature. From Fig. 1(d), the thickness of the film is estimated to be about 750 nm. In conclusion, with increasing deposition temperature, the size of ZnO nanorods increases and the ZnO films become more compact.

Fig. 2 shows XRD patterns of the ZnO films. Diffraction peaks with $2\theta = 31.8°, 34.4°, 36.2°, 47.5°, 56.6°, 62.8°, 67.8°$ are observed in the XRD patterns. These peaks are improved to be the (1 0 0), (0 0 2), (1 0 1), (1 0 2), (1 1 0), (1 0 3) and (1 1 2) diffractions of the hexagonal wurtzite ZnO (JCPDS card No. 36-1451), and no peaks from other impurities are detected. This indicates that all the prepared ZnO films are single hexagonal wurtzite ZnO phase.

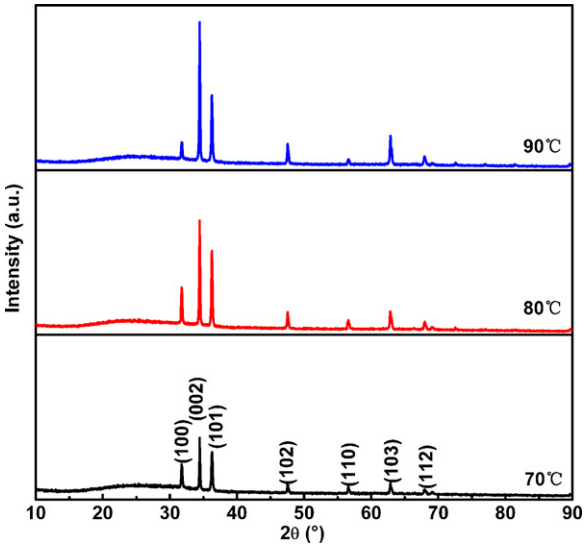

Fig. 2. XRD patterns of the ZnO films deposited at different temperatures for 1 h.

The formation process of ZnO films can be understood by the following reactions [11]:

$$Zn(NO_3)_2 \rightarrow Zn^{2+} + 2NO_3^- \quad (1)$$

$$(CH_3)_2NHBH_3 + H_2O \rightarrow BO_2^- + (CH_3)_2NH + 7H^+ + 6e^- \quad (2)$$

$$NO_3^- + H_2O + 2e^- \rightarrow NO_2^- + 2OH^- \quad (3)$$

$$Zn^{2+} + 2OH^- \rightarrow Zn(OH)_2 \quad (4)$$

$$Zn(OH)_2 \rightarrow ZnO + H_2O \quad (5)$$

The XRD results also show that the ZnO films have a *c*-axis preferred orientation. With the increase of deposition temperature, the intensity of diffraction peaks increases, which indicates that higher deposition temperature results in better crystallinity of the ZnO films.

To further prove the (0 0 2) preferred growth, texture coefficient (TC) was calculated from the X-ray data. TC represents the texture of the particular plane, deviation of which from unity implies the preferred growth. The different texture coefficient TC (hkl) can be calculated from the X-ray data using the well-known formula [13]:

$$TC(hkl) = \frac{I(hkl)/I_0(hkl)}{N^{-1}\sum_n I(hkl)/I_0(hkl)} \quad (6)$$

where $I(hkl)$, $I_0(hkl)$, N and n are the measured relative intensity of a plane (hkl), the standard intensity of the plane (hkl) taken from the JCPDS data, the reflection number and the number of diffraction peaks, respectively. The value of the texture coefficient indicates the maximum preferred orientation of the films along the diffraction plane. In other words, the TC value means that the increase in

Table 1
TC values of (002), (100) and (101) planes for ZnO films prepared at different temperatures.

	Temperature		
	70 °C	80 °C	90 °C
TC (002)	1.67	1.81	2.20
TC (100)	0.79	0.63	0.34
TC (101)	0.54	0.56	0.46

Table 2
Resistivities of ZnO films under different cooling conditions.

	Cooling condition			
	As-grown	In furnace	In air	At −15 °C
Resistivity (Ω cm)	>150	27.9	9.98	0.525

preferred orientation is associated with increase in the number of grains along that plane.

Table 1 summarizes the texture coefficient (TC) of three crystal orientations, such as (002), (100) and (101) plane for the ZnO films. Among all the crystal orientations, the TC of (002) plane has the highest value. With increasing deposition temperature, TC of (002) plane increases. The films deposited at 90 °C show the highest TC = 2.20 for (002) plane. The results indicate that higher temperature is helpful for (002) preferred growth.

Table 2 lists the resistivity of the ZnO films under different cooling conditions. From Table 2, we can see that the resistivity decreases gradually with increasing cooling rate and a lowest resistivity of 0.525 Ω cm has been obtained, which is a little higher than Al-doped ZnO prepared by sol–gel method [14]. The improvement of the conductivity is due to the increasing carrier mobility and the decrease of grain boundary scattering resulted from a higher crystallinity after annealing. Additionally, the decrease of resistivity may also relate to the density of oxygen vacancies in the films which is influenced by the cooling rates. Oxygen vacancies can be introduced both from the crystal growth process and from the oxygen atoms escaping from the films at high temperatures.

The balanced concentration of oxygen vacancies under temperature T is described as follows:

$$C = N_{\text{sites}} \exp\left(-\frac{E^{\text{f}}}{k_B T}\right) \quad (7)$$

where N_{sites} stand for the concentration of sites where the defects can occupied. E^{f} is related to chemical potentials of zinc, oxygen and zinc oxide which depend on the growth conditions, k_B is Boltzmann's constant, and T is the temperature.

According to Eq. (7), with the increase of the annealing temperature, the concentration of oxygen vacancies increases. After annealing at 500 °C for 1 h, a high concentration of oxygen vacancies in the ZnO films formed. Then the films are cooled down rapidly from 500 °C to room temperature. In this process, the oxygen vacancies could be "frozen" and kept in the films to room temperature. In other words, more oxygen vacancies in ZnO films are obtained by rapid cooling. Therefore, the concentration of the oxygen vacancies is larger for ZnO film cooled at −15 °C than that of ZnO films cooled in other manners. The increase of the carrier concentration results in the increase of the conductivity for ZnO film cooled at −15 °C.

Fig. 3(a) shows the normalized PL spectra of the ZnO films. The peak around 380 nm is attributed to band-edge emission, which corresponds to recombination of free-excitons. The broad PL emission in the visible range is attributed to the oxygen defect [15,16]. Compare with the annealed films, the PL spectra of the unannealed film exhibits the weakest visible light emission. With increasing cooling rate, the intensity of the PL in the visible range becomes stronger. The ZnO film cooled at −15 °C shows the strongest emission in the visible range. In order to further study the effects of oxygen vacancies on the PL in the visible range, the PL spectra within the wavelength range of 440–650 nm are fitted using two Gaussians curves centered at wavelengths of 535 nm (2.32 eV) and 596 nm (2.08 eV). The two superposition peaks locate in the green and yellow ranges, respectively. A typical deconvolution of a PL spectrum in terms of these two contributions is shown in Fig. 3(b) for the ZnO films after background subtraction. Table 3 summarizes the fitting parameters, peak positions, area, full width at half maximum (FWHM) for the films. Many researchers have reported the green and yellow emissions in ZnO [17–22]. Most of the literatures reported that the yellow emission can attribute to interstitial oxygen [20,21]. Vanheusden et al. [16] and Wang et al. [22] reported that oxygen vacancies are responsible for the green emission in ZnO. As shown in Table 3, with increasing cooling rate, area of green and yellow emissions increases. The increase of the emissions is

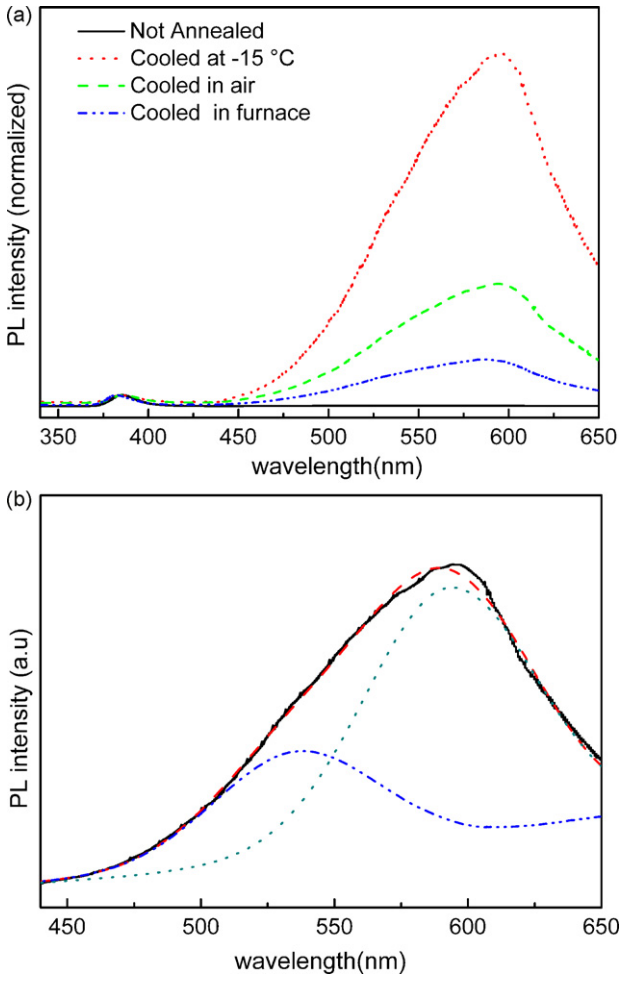

Fig. 3. (a) The normalized room-temperature PL spectra of all films. (b) The Gaussians fitting result of the room-temperature PL spectra for ZnO films cooling at −15 °C.

Table 3
Fitting results from PL spectra of ZnO films.

Cooling condition	Peak 1			Peak 2		
	Peak (nm)	FWHM (nm)	Area	Peak (nm)	FWHM (nm)	Area
In furnace	535	76.7	151	593	69.7	229
In air	535	75.7	312	593	72.7	623
At −15 °C	535	72.8	780	593	74.6	1901

attributed to the increase of oxygen vacancies and interstitial oxygen in the ZnO films, oxygen vacancies and interstitial oxygen of the ZnO films originating from annealing at high temperature is kept in the films, when cooling down to room temperature. Therefore, with the increase of the cooling rate, the concentration of oxygen vacancies increases. The results are consistent with that of obtained regarding the electrical properties.

4. Conclusions

The single-phase hexagonal wurtzite ZnO films are prepared on the Ag-coated glass substrate by wet chemical method at different deposition temperatures. With the increasing deposited temperature, the size of ZnO nanorods, the compaction degree of the ZnO films and the *c*-axis preferred orientation increase.

With the increase of cooling rate, the conductivity of the films is greatly improved and the PL intensity in visible range becomes stronger. The increase of the conductivity and the enhanced PL intensity in green energy range are attributed to the increase of oxygen vacancies in the films.

Acknowledgments

This work was financially supported by the Key grant Project of Chinese Ministry of Education (Grant No. 309027), and partially by the National Science Fund for Distinguished Young Scholars (Grant No. 50925103).

References

[1] R. Könenkamp, R.C. Word, C. Schlegel, Appl. Phys. Lett. 85 (2004) 6004.
[2] W.I. Park, J.S. Kim, G.C. Yi, M.H. Bae, H.J. Lee, Appl. Phys. Lett. 85 (2004) 5052.
[3] J.B. Baxter, E.S. Aydil, Appl. Phys. Lett. 85 (2005) 053114.
[4] Z. Fan, J.G. Lu, Appl. Phys. Lett. 86 (2005) 123510.
[5] Z.L. Wang, Mater. Today 7 (2004) 26.
[6] Y.E. Lee, J.B. Lee, Y.J. Kim, H.K. Yang, J.C. Park, H.J. Kim, J. Vac. Sci. Technol. A 14 (1996) 1943.
[7] V. Craciun, J. Elders, J.G.E. Gardenievs, I.W. Boyd, Appl. Phys. Lett. 65 (1994) 2963.
[8] Y. Natsume, H. Sakata, T. Hirayama, Phys. Status. Solidi A 148 (1995) 485.
[9] K. Ogata, K. Sakurai, Sz. Fujita, Sg. Fujita, K. Matsushige, J. Cryst. Growth 214 (2000) 312.
[10] Y. Natsume, H. Sakata, Thin Solid Films 372 (2000) 30.
[11] M. Izaki, J. Electrochem. Soc. 144 (1997) L3.
[12] Q. Tian, J.G. Li, Q. Wang, S. Wang, X. Zhang, Thin Solid Films 518 (2009) 313.
[13] C.S. Barret, T.B. Massalski, Structure of Metals, Pergamon Press, Oxford, 1980.
[14] Y.S. Kim, W.P. Tai, Appl. Surf. Sci. 253 (2007) 4911.
[15] Z.M. Liao, H.Z. Zhang, Y.B. Zhou, J. Xu, J.M. Zhang, Phys. Lett. A 372 (2008) 4505.
[16] K. Vanheusden, W.L. Warren, C.H. Seager, D.R. Tallant, J.A. Voigt, B.E. Gnade, J. Appl. Phys. 79 (1996) 7983.
[17] A.B. Djurišić, Y.H. Leung, K.H. Tam, L. Ding, W.K. Ge, W.K. Chan, Nanotechnology 18 (2007) 095702.
[18] Y.H. Leung, A.B. Djurišić, Z.T. Liu, D. Li, M.H. Xie, J. Phys. Chem. Solids 69 (2008) 353.
[19] L.E. Greene, M. Law, J. Goldberger, F. Kim, J.C. Johnson, Y. Zhang, R.J. Saykally, P. Yang, Angew. Chem. Int. Ed. 42 (2003) 3031.
[20] X.L. Wu, G.G. Siu, C.L. Fu, H.C. Ong, Appl. Phys. Lett. 78 (2001) 2285.
[21] Y.G. Wang, S.P. Lau, X.H. Zhang, H.W. Lee, S.F. Yu, B.K. Tay, H.H. Hng, Chem. Phys. Lett. 375 (2003) 113.
[22] M. Wang, C.H. Ye, Y. Zhang, G.M. Hua, H.X. Wang, M.G. Kong, L.D. Zhang, J. Cryst. Growth 291 (2006) 334.